

Subglacial drainage characterization: Supplementary material

Camilo Rada and Christian Schoof

Department of Earth, Ocean and Atmospheric Sciences, University of British Columbia, 2207 Main Mall, Vancouver, BC Canada.

Correspondence to: Camilo Rada (camilo@rada.cl)

1 Model continuum formulation

The discrete element model of the main text is easy in principle to generalize to a coupled sheet-network model as in Werder et al. (2013). Instead of our conduits S_K , the model represents cavity-like conduits in averaged way as a sheet with thickness h . The ‘sheet’ formulation of our discrete element model would be

$$5 \quad -v_p \frac{\partial N}{\partial t} + \frac{\partial h}{\partial t} + \nabla \cdot \mathbf{q} = m \quad (1a)$$

$$\frac{\partial h}{\partial t} = u_b(h_r - h)/l_r - c_2 h |P_e|^{n-1} P_e \quad (1b)$$

$$\mathbf{q} = \kappa \max(h - h_p, 0)^\alpha |\nabla \phi|^{\beta-2} \nabla \phi + \kappa_{\text{leak}} \nabla \phi \quad (1c)$$

$$\phi = \rho_i g s + (\rho_w - \rho_i) g b - N \quad (1d)$$

$$P_e(x, y, t) = \int_{\Omega} G(x, y, x', y') N(x', y', t) dx' dy', \quad (1e)$$

10 which, with some minor notational changes, is the same as the Werder et al. (2013) if we put $h_p = 0$ and $G(x, y, x', y') = \delta(x - x')\delta(y - y')$. Here v_p , h_r , l_r , c_2 , κ , h_p and κ_{leak} are constants equivalent to V_p , h_K , S_{K0} , c_2 , c_3 , S_{PK} and k_{leak} in the discrete element model, with l_r/n_c representing an averaging length scale for turning the discrete model into its continuum counterpart. In particular, h_p is the percolation cut-off discussed in the main paper, while G is the continuum version of the discrete averaging kernel G_{ijk} , and we require that $G \geq 0$, $\int_{\Omega} G(x, y, x', y') dx' dy' = 1$ for all (x, y) .

15 At this point, the need for an averaging term when computing creep closure may still seem vague, beyond the previously stated need to account for discontinuities in N that can evolve once h drops below the percolation cut-off: when such discontinuities arise, we would expect the closure of one cavity (that is, the viscous flow of ice around the cavity) to be affected not just by the difference between overburden and water pressure in that single cavity (as is the case in models in which water pressure is the same in all cavities, see Fowler (1986), Schoof (2005) and Gagliardini et al. (2007)), but also by water pressure

20 in other nearby cavities. Effectively, we expect the normal stress transfer effect that we appeal to in order to explain anticorrelated borehole water pressures (see also Murray and Clarke, 1995) to affect cavity creep closure rates. An averaging kernel represents a simple way of attempting to capture this effect, although a more detailed process understanding is certainly a key area for future research.

Practically, the need for some kind of non-local closure is actually easier to understand in the continuum rather than the discrete setting. Take a point (x, y) at which $h < h_p$ and assume that leakage allowed by κ_{leak} is negligible; there is then no water flow at that location. Suppose also that there is no distributed water supply, which would make the persistence of hydraulically isolated patches of bed difficult to maintain. In other words, put $m = 0$. Suppose also that we simply set $P_e = N$.

5 We would obtain a pair of evolution equation for water pressure

$$-v_p \frac{\partial N}{\partial t} + u_b(h_r - h)/l_r - c_2 h |N|^{n-1} N = 0.$$

$$\frac{\partial h}{\partial t} = u_b(h_r - h/l_r) - c_2 h |N|^{n-1} N.$$

As pointed out by Hoffman et al. (2016), changes in borehole water pressure can now result from temporal variations in ice flow u_b imposed by effective pressure changes elsewhere at the bed. However, in the absence of such imposed sliding velocity variations, the evolution equations for h and N become purely local, and do not couple with the rest of the bed. In particular, if at the point of close-off N was large enough to be causing net closure (so $\partial h / \partial t < 0$ at that point, as required to be entering a closed-off state), it is relatively straightforward to show that close-off will never be reversed, in the sense that h will not rise above h_p again.

The model above excludes the effect of overpressurization discussed by Schoof et al. (2012), Hewitt et al. (2012) and Tsai and Rice (2010). While overpressurization undoubtedly contributes to the establishment of hydraulic connections in parts of the season (and we suspect that the spring event in particular may be partly driven by overpressurization) our data set indicates reconnection events that occur when water pressure is significantly below overburden. In terms of modelling, we are therefore faced with two possibilities: either reconnection is driven purely by ice motion (changes in u_b) or ongoing leakage (so κ_{leak} is not negligible), or changes in water pressure near a given location can drive changes in cavity evolution and connectivity. The averaging kernel G is intended to allow for the latter possibility.

Werder et al. (2013) couple their sheet model to a conduit network model that allows for channelization. It is straightforward also to generalize that model component to our percolation cut-off, by writing

$$\frac{\partial S}{\partial t} = c_1 Q \frac{\partial \phi}{\partial s} + l_c \mathbf{q} \cdot \mathbf{t} \frac{\partial \phi}{\partial s} - c_s S |P_e|^{n-1} P_e \quad (1f)$$

$$Q = c_3 \max(S - S_{PR}, 0)^\alpha \left| \frac{\partial \phi}{\partial s} \right|^{\beta-2} \frac{\partial \phi}{\partial s} \quad (1g)$$

$$25 \quad \frac{\partial S}{\partial t} + \frac{\partial Q}{\partial s} = \frac{\rho_i}{\rho_w} c_1 Q \frac{\partial \phi}{\partial s} \quad (1h)$$

where s is the arc length coordinate along the conduit and \mathbf{t} the unit tangent vector in the direction of increasing s , and all quantities are evaluated at the channel location. S replaces the earlier variable S_R , and S_{PR} is the relevant percolation cut-off. At nodes of the network, there may be additional volume storage and water input as described Werder et al. (2013).

While the simple transcription of the earlier model in Werder et al. (2013) to a percolation cut-off is relatively straightforward, it is not devoid of deeper modelling issues. Defining the closure term P_e non-locally in particular makes the identification of (1a) as “parabolic” in the variable N questionable: the non-local closure term is not monotone in the usual sense (Ekeland

and Temam, 1976), while the diffusion term can vanish on part of the domain. In particular, substituting for $\partial h/\partial t$ in (1a), replacing $N = \phi_0 - \phi$ with $\phi_0 = \rho_i g s + (\rho_i - \rho_w) g b$, multiplying by a test function θ and integrating over the domain yields the weak form

$$\int_{\Omega} v_p \theta \frac{\partial \phi}{\partial t} + \kappa_0 \max(h - h_p, 0)^\alpha |\nabla \phi|^{\beta-2} \nabla \phi \cdot \nabla \theta \, d\Omega + \int_{\Omega} u_b (h_r - h) / l_r \theta - c_2 h |P_e|^{n-1} P_e \theta - m \theta \, d\Omega + \int_{\partial\Omega} \mathbf{q} \cdot \mathbf{n} \, d\Gamma = 0,$$

where \mathbf{n} is the outward-pointing unit normal to domain. Isolating the non-local closure term as

$$\langle A\phi, \theta \rangle = \int_{\Omega} -c_2 h |P_e|^{n-1} P_e \theta \, d\Omega$$

where
$$P_e(x, y, t) = \int_{\Omega} G(x, y, x', y') [\phi_0(x', y') - \phi(x', y', t)] \, dx' dy',$$

there appears to be no obvious reason, even with the stipulations that $G \geq 0$, $\int_{\Omega} G(x, y, x', y') \, dx' dy' = 1$, that we should always have monotonicity in the sense that

$$\langle A\phi - A\theta, \phi - \theta \rangle \geq 0$$

for all functions θ, ϕ .

- 5 While this observation may seem a technicality from the modelling perspective, probably mostly relevant to the numerical solution of the problem, the non-local definition of closure has more significant implications when we try to adapt the model for overpressurization as is done in Schoof et al. (2012) and Hewitt et al. (2012). The formulation in these papers relies on ice being able to separate from the bed when the effective pressure driving the closure term $c_2 h |P_e|^{n-1} P_e$ vanishes; rather than requiring negative effective pressure to enlarge the ice-bed gap, the model then allows the gap evolution to be dictated by the
- 10 evolution of water depth, identifying the two with each other. At the same time, the extended model of Schoof et al. (2012) and Hewitt et al. (2012) also permits water and ice to separate where water pressure drops to zero. In their model formulation, $P_e = N$ and it is impossible for effective pressure and water pressure to vanish at the same time, which is essential for their model formulation. With a non-locally defined effective pressure P_e , this does become at least a theoretical possibility: we expect that ice-bed separation occurs when $P_e = 0$, which can in principle occur at the same time as N reaching the value
- 15 $\rho_i g(s - b)$ required for water pressure to drop to zero; in that case, we could have full ice-bed separation with the gap between the two not filled completely by water, but at least partially by air. In the models of Schoof et al. (2012) and Hewitt et al. (2012), this would however leave the rate of change of the ice-bed gap indeterminate.

- This possibility strongly suggests that, at least if we are to model partial flotation of the ice, a more careful approach to non-local closure of the sheet is required, possibly based on a more detailed study of cavity opening and closing in situations
- 20 where cavities can become closed off from each other and water pressure may differ from cavity to cavity. Such partial flotation may be essential in explaining the formation of an active drainage system in the early melt season, especially if it is possible for drainage connections to close off completely over winter.

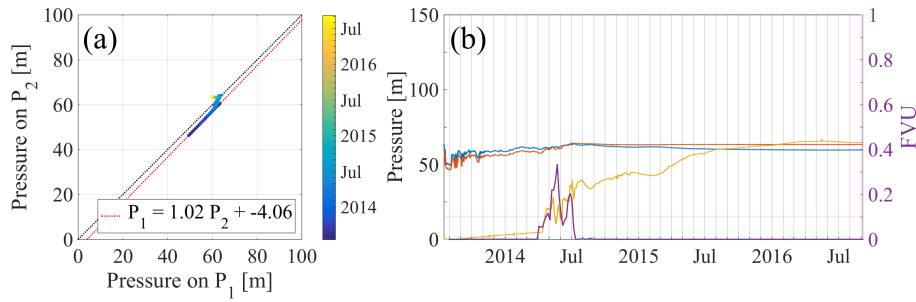


Figure 1. Pressure records P_1 and P_2 for the two sensors in borehole 13H16, installed 20 cm apart. (a) A phase plot with points colour-coded by time. The expected relationship $P_1 = P_2$ is shown as a black dotted line. The linear regression model constructed over the first month after installation is shown as a red dotted line, with parameter values given in inset box. (b) Pressure time series for P_1 (blue) and P_2 (orange). The residual between P_2 and the linear regression model is shown in yellow, scaled by a factor of 10 for visibility. Unexplained variance over a one-month moving window is shown as a purple line.

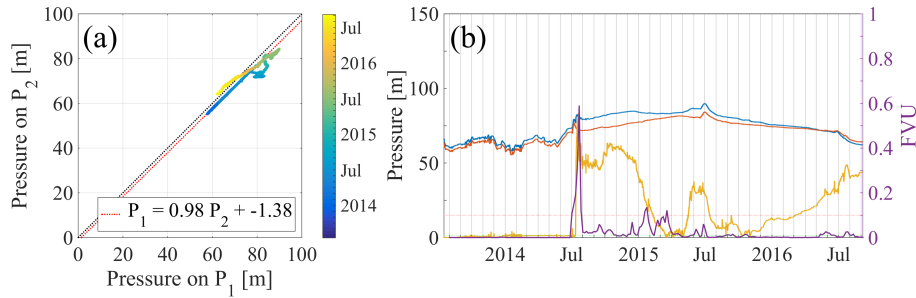


Figure 2. Pressure records for the two sensors in borehole 13H17, installed 34 cm apart, plotted using the same scheme as in Fig. 1

2 Doubly instrumented boreholes: a test of pressure measurement reliability

The analysis of the pressure records from South Glacier presented in this paper does not rely in the accuracy of absolute pressure values, in the sense that we have not attempted to use the difference between water pressures recorded in different holes as an indication of hydraulic potential gradients: if a sensor is incorrectly calibrated and, for instance, the amplitude of recorded diurnal pressure oscillations is computed incorrectly as a result, our interpretation of connection between boreholes would be unaltered in sections 3.2 and 3.4 of the main paper: unless the calibration coefficients are wildly incorrect, variations in the amplitude of diurnal oscillation over a longer periods of time will still resemble each other even if the computed pressure difference between the boreholes varies spuriously. However, we do rely on the true calibration parameters being stable over time, so that for instance inferred variations in the amplitude of diurnal oscillations are not caused by calibration drift but by the actual response of the drainage system to surface forcing. Similarly, we rely on calibration coefficients being stable in order to infer whether isolated boreholes experience a seasonal drift in water pressure during summer in section 3.4.

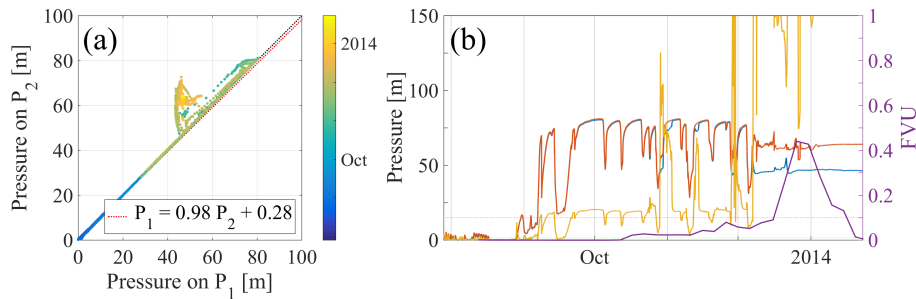


Figure 3. Pressure records for the two sensors in borehole 13H58 (the “fast-flow” borehole of the main paper), installed 70 cm apart, plotted using the same scheme as in Fig. 1.

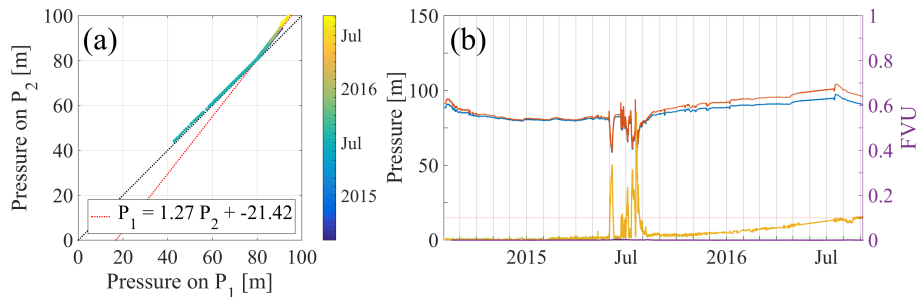


Figure 4. Pressure records for the two sensors in borehole 14H60, installed 20 cm apart. P_2 was recorded by a digital sensor. The plotting scheme used is the same as in Fig. 1.

As described in section 3.6, we instrumented eleven boreholes with two sensors to assess the stability of calibration parameters and the overall reliability of sensors as they remain in the glacier over extended periods of time. All pressure sensors used in the study (see section 2) provide a differential voltage output that varies nearly linearly with pressure. Therefore, a linear calibration is used to compute pressure values from raw voltage readings,

$$P = MV - P_0, \quad (2)$$

where P is the pressure at the sensor, V the voltage measured, P_0 the offset (corresponding to the voltage measured at atmospheric pressure), and M is the multiplier.

In panel a of each of Figs. 1–11 shows the pressure at one sensor in a given borehole, computed using pre-deployment calibration values of M and P_0 , against the corresponding value for the other sensor in the same borehole, for all doubly-instrumented boreholes. If, as one would expect, both sensors record the same pressure (the expected hydrostatic pressure difference between the two sensors being minimal except perhaps in figure 3, then these phase plots should lie along the black dotted line $P_2 = P_1$. However, there are usually small errors in the calibration parameters, which we estimate by a linear regression over the data recorded during the first month after installation (red dotted line). Deviations from that line indicate

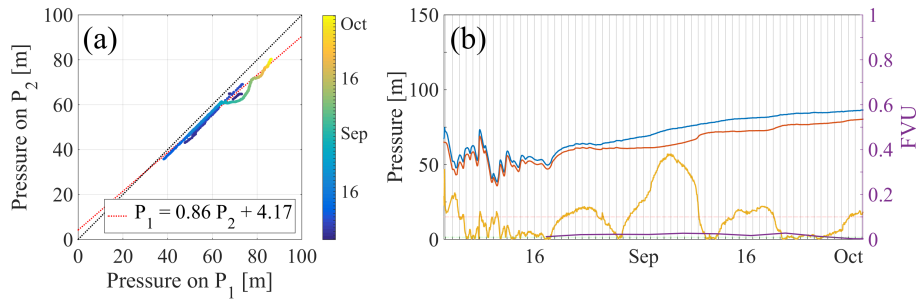


Figure 5. Pressure records for the two sensors in borehole 14H62, installed at the same elevation. P_2 was recorded by a digital sensor. The plotting scheme used is the same as in Fig. 1.

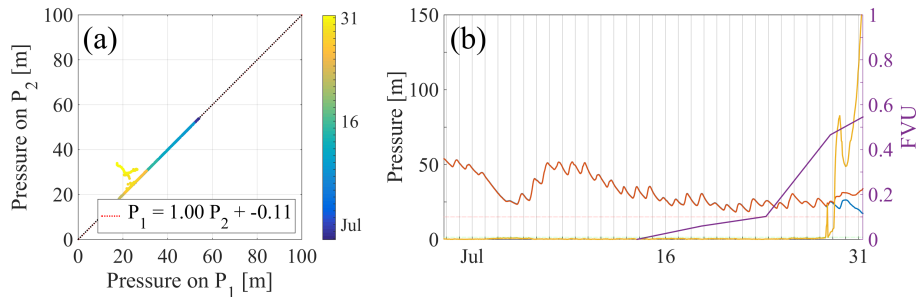


Figure 6. Pressure records for the two sensors in borehole 15HL07, installed at the same elevation. The plotting scheme used is the same as in Fig. 1.

that one or both of the sensors is not behaving linearly as in equation 2, or that the two sensors have become isolated from each other due to freezing or ice creep.

In panel b of each figure the pressure recorded at each sensor is presented (blue and orange lines) as computed from pre-installation calibration. Also plotted is the difference between the recorded pressures that would remain if instead of using pre-deployment calibration values, we also applied the linear regression model over the first month of sensor operation indicated in the inset in panel a. This residual is multiplied by a factor of 10 for easier visibility, and plotted as a yellow line, with a 10x.

To quantify changes in the similarity of both records, we have also computed linear regressions over moving one-month windows, and subsequently calculated the fraction of unexplained variance (FUV) over that period. The FUV is the fraction of the variance in P_2 that can not be explained by variations in P_1 . As such, it is a measure of the quality of a linear fit: if samples are taken at times t_1, t_2, \dots, t_N the FUV would be

$$FUV = \frac{\sum_{i=1}^N (P_1(i) - P'_2(i))^2}{\sum_{i=1}^N (P_1(i) - \mu_1)^2} \quad (3)$$

where $P_1(i)$ is the value of P_1 at time t_i , $P'_2(i)$ is the value of P_2 at time t_i , transformed linearly using regression model over the moving one-month window. N is the number of samples in the window and μ_1 is the mean of P_1 .

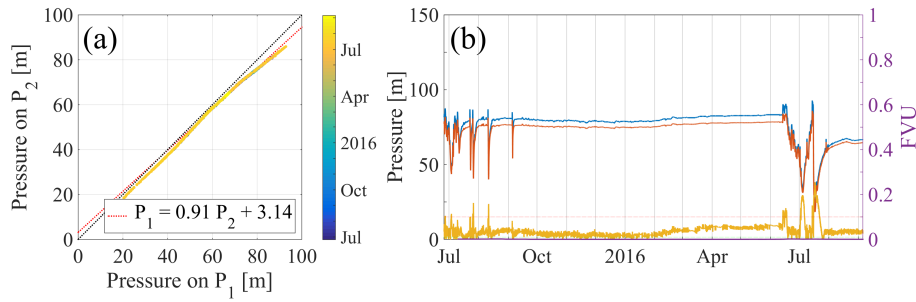


Figure 7. Pressure records for the two sensors in borehole 15HU01, installed at the same elevation. P_2 was recorded by a digital sensor. The plotting scheme used is the same as in Fig. 1.

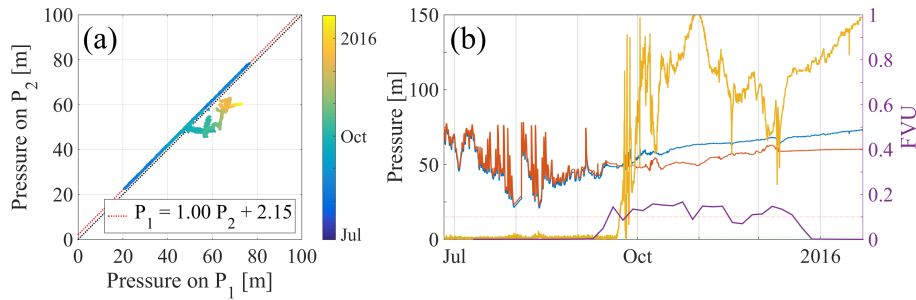


Figure 8. Pressure records for the two sensors in borehole 15HU04, installed at the same elevation. P_2 was recorded by a digital sensor. The plotting scheme used is the same as in Fig. 1.

We see that with the exception of Fig. 4, all differences in the pressure are smaller than 5 meters, and deviations in the multiplier (the difference between coefficient of P_1 in the formula in panel a and the expected value of one) are in most cases smaller than 2%. For figures 4 and 7, where anomalously large slopes are observed, we can see that there is a clear change in the slope below a certain pressure, suggesting that the sensors used most likely did not behave linearly over their nominal calibration pressure range. A similar effect probably affects the sensors in Fig. 5, where the two sensors may have also become disconnected from each other. In all cases, the non-linearity seems to occur only the digital sensors used, and these make up a small fraction of the whole data set.

In the first month of each time series, the residual remains below 5 meters and the FUV below 1%. Such consistent records can extend for more than one year (Fig. 7), but agreement between the sensors can also degrade after few months. The increase in the residual usually starts at a very specific point in time. This is suggestive of a loss of connection between the two sensors. Some examples of possible disconnection are evident in Fig. 2 in July 2014, in Fig. 3 in December 2013, Fig. 6 in late July 2015, and Fig. 9 in October 2015. It is unlikely that the difference observed in these cases arise from a single, transient high-pressure spike changing the calibration of the sensor instantly: the pressure records should then still be linearly related to each other, but with different offsets and multipliers, and the FUV should remain small.

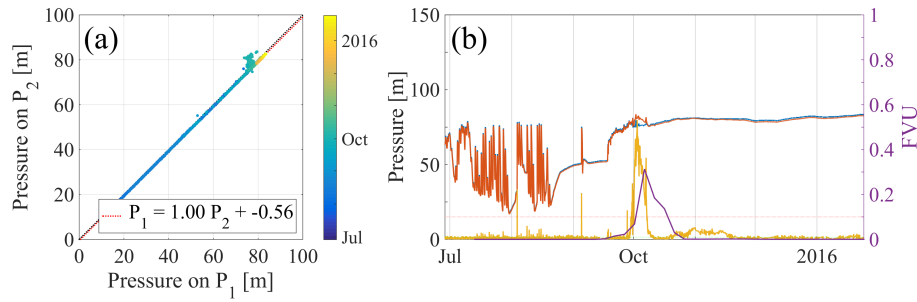


Figure 9. Pressure records for the two sensors in borehole 15HU05, installed at the same elevation. P_2 was recorded by a digital sensor. The plotting scheme used is the same as in Fig. 1.

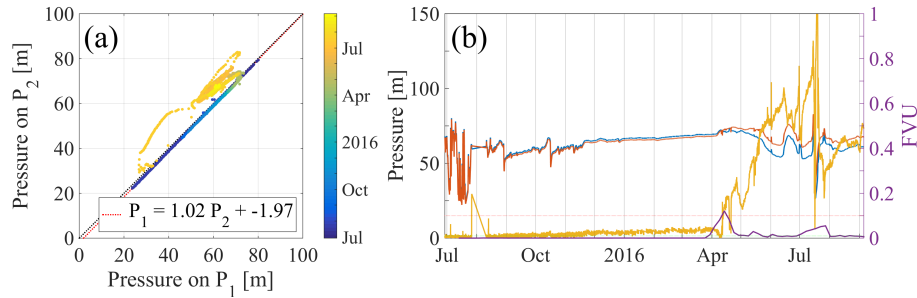


Figure 10. Pressure records for the two sensors in borehole 15HU17, installed at the same elevation. P_2 was recorded by a digital sensor. The plotting scheme used is the same as in Fig. 1.

A few records (for instance those in Figs. 1 and 5) are consistent with a gradual change on the offset and/or multiplier. However, this effect seem to be small in comparison with the differences arising from possible disconnection. As described in section 3.6 and Fig. 15 of the main text, disconnection can be explained by sensors becoming encased in ice due to ice creep or, less likely due to radar measurements indicating temperate basal ice, due to freezing. Ice creep is consistent as an explanation for disconnections with most disconnections happening after the end of the summer drainage season, and happening sooner in sensor pairs that are recording consistently lower water pressures (for instance Fig. 6); the ice surrounding the corresponding boreholes should be subject to higher creep rates. It is important to note that residuals and FUV are typically very small over periods where diurnal variations are present, and that significant inconsistencies between sensor pairs in the same borehole appear in the absence of such variations, indicating a loss of connection to the drainage system.

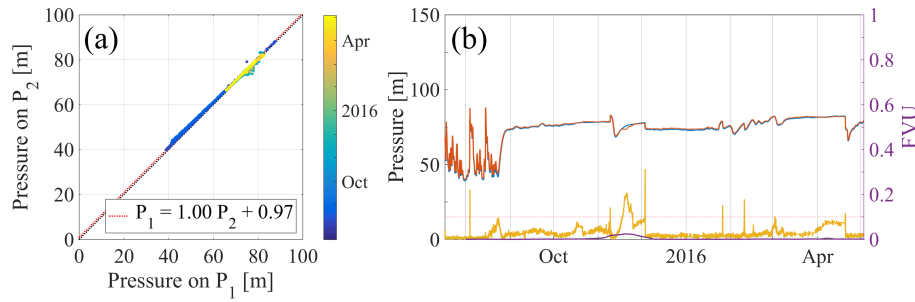


Figure 11. Pressure records for the two sensors in borehole 15HU50, installed at the same elevation. P_2 was recorded by a digital sensor. The plotting scheme used is the same as in Fig. 1.

References

- Ekeland, I. and Temam, R.: *Convex Analysis and Variational Problems*, North-Holland, Amsterdam, 1976.
- Fowler, A.: A sliding law for glaciers of constant viscosity in the presence of subglacial cavitation, *Proc. R. Soc. Lond. A*, 407, 147–170, 1986.
- 5 Gagliardini, O., Cohen, D., Råback, P., and Zwinger, T.: Finite-element modeling of subglacial cavities and related friction law, *J. Geophys. Res.*, 112, doi:10.1029/2006JF000576, 2007.
- Hewitt, I., Schoof, C., and Werder, M.: Flotation and free surface flow in a model for subglacial drainage. Part 2. Channel flow, *J. Fluid Mech.*, 702, 157–187, 2012.
- Hoffman, M., Andrews, L., Price, S., Catania, G., Neumann, T., Lüthi, M., Gulley, J., Ryser, C., Hawley, R., and Morriss, B.: Greenland subglacial drainage evolution regulated by weakly connected regions of the bed, *Nature Communications*, 7, 13903, doi:10.1038/ncomms13903, 2016.
- 10 Murray, T. and Clarke, G.: Black-box modeling of the subglacial water system, *Journal of Geophysical Research*, 100, 10 219–10 230, 1995.
- Schoof, C.: The effect of cavitation on glacier sliding, *Proceedings of the Royal Society of London A: Mathematical, Physical and Engineering Sciences*, 461, 609–627, doi:10.1098/rspa.2004.1350, <http://rspa.royalsocietypublishing.org/content/461/2055/609>, 2005.
- 15 Schoof, C., Hewitt, I., and Werder, M.: Flotation and free surface flow in a model for subglacial drainage. Part 1. Distributed drainage, *J. Fluid Mech.*, 702, 126–156, 2012.
- Tsai, V. and Rice, J.: A model for turbulent hydraulic fracture and application to crack propagation at glacier beds, *Journal of Geophysical Research: Earth Surface*, 115, doi:10.1029/2009JF001474, f03007, 2010.
- Werder, M., Hewitt, I., Schoof, C., and Flowers, G.: Modeling channelized and distributed subglacial drainage in two dimensions, *J. Geophys. Res.*, 118, 2140–2158, 2013.
- 20